

1 On the usefulness of four in vitro  
2 methods in assessing the intraluminal  
3 performance of poorly soluble, ionisable  
4 compounds in the fasted state  
5

6 Patrick J. O'Dwyer<sup>a,b,c</sup>, Karl J. Box<sup>a</sup>, Georgios Imanidis<sup>d,e</sup>, Maria Vertzoni<sup>b</sup>, Christos Reppas<sup>b\*</sup>

7  
8 a) Pion Inc. (UK) Ltd., Forest Row, East Sussex, UK

9 b) Department of Pharmacy, School of Health Sciences, National and Kapodistrian University of  
10 Athens, Zografou, Greece

11 c) School of Pharmacy, University College Cork, College Road, Cork, Ireland

12 d) University of Applied Sciences Northwest. Switzerland. School of Life Sciences, Institute of  
13 Pharma Technology, Hofackerstrasse 30, 4132 Muttenz, Switzerland

14 e) University of Basel, Department of Pharmaceutical Sciences, Basel, Switzerland  
15  
16  
17

18 \*To whom correspondence should be addressed:

19 **Christos Reppas PhD, Department of Pharmacy, School of Health Sciences, National and**  
20 **Kapodistrian University of Athens, Panepistimiopolis, 157 71 Zografou, Greece**

21 **Tel. 00 30 210 727 4678 / Fax: 00 30 210 727 4027 / reppas@pharm.uoa.gr**  
22

## 23 1. Introduction

24 Oral drug absorption is a complex process which can be influenced by many factors. These can be  
25 related to the underlying physiology of the gastrointestinal (GI) tract, the properties of the drug  
26 molecule and the drug formulation behaviour. These factors directly affect the absorption of drug  
27 and, therefore, its bioavailability. The appropriate use of *in vitro* tools is a critical challenge for the  
28 pharmaceutical industry when evaluating the oral absorption of new drugs. Obtaining biorelevant  
29 information on the performance of formulations can reduce the cost of drug development, decrease  
30 the amount of *in vivo* studies required and cut the time taken to reach the market. Various small-  
31 and full-scale *in vitro* methods to assess the luminal performance of solid drug products have been  
32 proposed, however, in many cases, their usefulness has not been fully explored (O'Dwyer et al.,  
33 2019). In addition, comparative evaluation of proposed *in vitro* methods from literature data is  
34 hindered by the use of different drug substances, formulations, and doses tested in the published  
35 studies.

36 In this study, we evaluated the usefulness of a small-scale two-stage biphasic system (Jankovic et al.,  
37 2019; O'Dwyer et al., 2020), a small-scale two-stage dissolution-permeation (D-P) system (O'Dwyer  
38 et al., 2020), the Erweka (Heusenstamm, Germany) mini-paddle apparatus, and the biorelevant  
39 gastrointestinal transfer (BioGIT) system (Kourentas et al., 2018) in assessing the intraluminal  
40 performance of poorly soluble, ionisable compounds in the fasted state. This assessment was  
41 completed either indirectly after incorporating *in vitro* data into physiologically based  
42 biopharmaceutics (PBB) models and simulating the plasma profiles (Jamei et al., 2020), or directly by  
43 comparing *in vitro* with luminal data. In this study, the luminal performance of formulations of two  
44 ionizable drug substances (diclofenac potassium and ritonavir) were examined. While the Erweka  
45 mini-paddle apparatus is considered to be a small-scale setup in previous works (Klein and Shah,  
46 2008), in pharmaceutical profiling and early formulation development an even smaller scale can be

47 beneficial. Therefore, in this article the Erweka mini-paddle apparatus is not categorised as a small-  
48 scale method, given the volume of water (250 mL) administered with a dose in clinical studies.

49 Diclofenac is a Biopharmaceutics Classification System (BCS) Class II weak acid (pKa 3.8) (Guhmann  
50 et al., 2013). The impact of formulation on the luminal performance of diclofenac potassium was  
51 appraised. Salts of low solubility weak acids may lead to precipitation of the free acid in the stomach  
52 due to pH-dependent solubility, with subsequent potential complications in the oral drug absorption  
53 process (Guhmann et al., 2013; Van Den Abeele et al., 2017, 2016). However, if the residence time in  
54 the stomach is short or rapid redissolution occurs in the intestine, precipitation may not be clinically  
55 significant. Two products containing the potassium salt of diclofenac were tested: an immediate-  
56 release tablet (Cataflam®) and powder for oral solution formulation (Voltfast®). *In vitro* data were  
57 used for the simulation of plasma profiles which were then evaluated versus previously published  
58 actual plasma data in adults (Marzo et al., 2000) or they were compared with previously published  
59 luminal data in adults (Van Den Abeele et al., 2017).

60 Ritonavir is a BCS class IV weak base (basic pKas = 1.8, 2.6) (Xu et al., 2017). The luminal performance  
61 of a ritonavir amorphous solid dispersion (ASD) tablet (Norvir®) was evaluated under conditions  
62 simulating normal and reduced gastric acid secretion in the fasted state. Due to the amorphous  
63 ritonavir state, supersaturation can occur in the stomach and, especially, in the increased pH of the  
64 lumen of the upper small intestine. The concept has been applied to various lipophilic weak bases  
65 (Brouwers et al., 2017; Litou et al., 2020; Xu et al., 2017) to achieve adequate oral bioavailability.  
66 However, supersaturated states are thermodynamically unstable and the degree of supersaturation  
67 is the driving force for precipitation (Brouwers et al., 2009; Hens et al., 2016; Psachoulias et al.,  
68 2011). As with diclofenac potassium, in this study *in vitro* ritonavir data were used for the simulation  
69 of plasma profiles which were then evaluated versus previously published actual plasma data in  
70 adults (Ng et al., 2008) or they were compared with previously published luminal data in adults (Van  
71 Den Abeele et al., 2020).

## 72 2. Materials and Methods

### 73 2.1. Materials

74 Diclofenac free acid (> 98.0 %) and diclofenac potassium (> 98.0 %) were received from Kemprotec  
75 (Cumbria, UK), to obtain the standard UV spectra for the *in situ* tests and for the standard curves.  
76 Cataflam® 50mg IR film-coated immediate release tablets (Novartis Ireland Limited, Dublin, Ireland),  
77 and Voltfast® 50mg powder for oral solution (Novartis Pharma Schweiz AG, Rotkreuz) were obtained  
78 from community pharmacy sources, with lot number and expiry dates provided in the  
79 Supplementary materials (Table S1). Both formulations contain 50 mg of diclofenac potassium,  
80 equivalent to 44.3 mg of the free acid.

81 Ritonavir (≥ 98 %) was obtained from Sigma-Aldrich (Dorset, UK). Norvir® 100mg film-coated tablets  
82 (AbbVie Deutschland GmbH & Co. KG, Ludwigshafen) was obtained from community pharmacy  
83 sources, with lot number and expiry dates provided in the Supplementary materials (Table S1).  
84 Norvir® film-coated tablet is an ASD in a polyvinylpyrrolidone – vinyl acetate copolymer matrix (Xu et  
85 al., 2017).

86 Acceptor Sink Buffer (ASB), consisting of a HEPES buffer at pH 7.4 along with surfactants, and GIT  
87 (Gastrointestinal Tract) Lipid Solution (20% lecithin in dodecane lipid solution) were received from  
88 Pion Inc (MA, USA). SIF powder and Fasted State Simulated Intestinal Fluid (FaSSIF) V2 (Bou-Chacra  
89 et al., 2017) powder were obtained from biorelevant.com (London, UK). Decanol was purchased  
90 from Alfa Aesar (Heysham, UK). Hard gelatin capsules (volume 0.37 mL, diameter 6.0 mm) were  
91 purchased from Agar Scientific Ltd (Essex, UK). All other chemicals and solvents were of analytical  
92 grade or HPLC grade and purchased from Fisher Scientific UK or Sigma-Aldrich, UK. All materials used  
93 in the study were within their expiry date when the experimental work was conducted.

94

95        2.2. *Methods*

96            2.2.1. Dose Selection

97 Dose selection was based on single dose and the water co-administered in the published clinical  
98 studies in adults i.e., 50 mg and 100 mg for diclofenac potassium and ritonavir, respectively,  
99 administered with 250 mL of water. In experiments with the small-scale systems, the dose was  
100 scaled down proportionally to the volume of aqueous media used in the corresponding system  
101 (experimental volume), as follows:

102                    
$$\text{Scaled down dose (mg)} = \frac{\text{Clinical dose (mg)} * \text{experimental volume (mL)}}{250 \text{ mL}}$$

103 As the small-scale two-stage biphasic system has an aqueous volume of 40 mL, the doses tested  
104 were 8 and 16 mg for the diclofenac potassium and ritonavir, respectively. For the small-scale two-  
105 stage D-P system, the doses were scaled according to the 20 mL donor chamber volume (i.e., 4 and 8  
106 mg for diclofenac potassium and for ritonavir, respectively). The diclofenac potassium and ritonavir  
107 tablets were crushed using a pestle and mortar to allow the scale down of the dose required for  
108 both small-scale setups. The downsized quantity of formulation then was weighed into a hard  
109 gelatin capsule.

110            2.2.2. Small-scale two-stage biphasic system

111 The methodology using the inForm (Pion Inc.) instrument was the same as outlined previously  
112 (Jankovic et al., 2019; O'Dwyer et al., 2020). Briefly, the relevant quantity of formulation was  
113 weighed into a hard gelatin capsule which was added into the system using the automated sample  
114 handling mechanism. The test consisted of two stages, representing the transition from gastric to  
115 intestinal conditions. The duration of the gastric and intestinal sectors were 30 and 210 minutes,  
116 respectively. Initially the dissolution media consisted of 36 mL of a 0.01 M acetate phosphate buffer  
117 at pH 2. After 30 minutes, 4 mL of 10 x concentrated Level II FaSSIF V2 was added into the  
118 dissolution vessel and a layer of decanol was added into the vessel. Stirring was temporarily halted  
119 and the decanol was added in a dropwise manner to reduce the risk of mixing with the aqueous  
120 layer. The pH of the aqueous media was then adjusted to 6.8, to represent the shift into intestinal

121 conditions. The pH transition occurred after addition of the decanol layer to facilitate absorption of  
122 drug in the critical period immediately after the shift, where drug substances may be highly  
123 supersaturated and liable to precipitate. pH was controlled to  $\pm 0.1$  pH unit of the target pH  
124 throughout the experiment by the instrument, adjusting using 0.5 M HCl or 0.5 M NaOH when  
125 necessary. Stirring was set to 100 rpm and the temperature was controlled to 37 °C. All experiments  
126 were carried out in triplicate. When simulating hypochlorhydric gastric conditions, the pH of the 0.01  
127 M acetate phosphate was set at pH 5 (Litou et al., 2016) during the gastric sector (buffer capacity at  
128 pH 5 = 4.8 mEq/pH/L)(Litou et al., 2016; Segregur et al., 2021, 2019). The 0.01M acetate phosphate  
129 buffer was selected as the instrument is calibrated to control the pH using this buffer.

### 130 2.2.3. Small-scale two-stage D-P system

131 The small-scale two-stage D-P system was based on the  $\mu$ FLUX system (Pion Inc.) as outlined  
132 previously (O'Dwyer et al., 2020). Briefly, the experiment consisted of two stages to mimic the  
133 transition from the stomach to the small intestine. The duration of the gastric and intestinal sectors  
134 were 30 and 210 minutes, respectively. Initially the donor chamber was filled with 15 mL of  
135 hydrochloric acid solution (pH 2) and the drug was manually introduced. After 30 minutes, 5 mL of 4  
136 x concentrated Level II FaSSIF V2 was added into the donor chamber. The resulting pH in the donor  
137 chamber was  $6.8 \pm 0.1$ , with further information on the phosphate buffer preparation provided in  
138 the Supplementary Materials (table S2). The acceptor chamber was filled throughout the  
139 experiment with ASB (20 mL). The two chambers were separated by a biomimetic membrane which  
140 consisted of 0.45 $\mu$ m polyvinylidene fluoride membrane coated with 25  $\mu$ L of the GIT lipid solution. The  
141 surface area of the membrane was 1.54 cm<sup>2</sup>. Stirring was provided by cross-bar magnetic stirrers in  
142 both chambers and was set at 150 rpm throughout the experiment. All experiments were carried out  
143 in triplicate. When simulating hypochlorhydric gastric conditions, the gastric media was a dilute  
144 hydrochloric acid solution (pH 5).

145           2.2.4. Erweka mini-paddle apparatus  
146 Erweka mini-paddle apparatus experiments were carried out using 250 mL volumes in a 500 mL  
147 capacity mini-vessel (Erweka) for all media tested. Stirring was set at 75 rpm for each experiment.  
148 Formulations were tested in a single medium throughout the experiment i.e., in Level III FaSSGF  
149 (fasted state simulated gastric fluid) and in Level II FaSSIF both at 37 °C (Markopoulos et al., 2015). In  
150 addition, the ritonavir ASD tablets were tested using Level III hypochlorhydric FaSSGF (Litou et al.,  
151 2017). Samples were filtered through a regenerated cellulose 0.45 µm filter (Titan 3, 17 mm,  
152 ThermoFisher, MA, USA). Adsorption of drug substances to the filter had been evaluated and found  
153 to be negligible in all cases.

154           2.2.5. BioGIT system  
155 BioGIT system experiments with the diclofenac formulations were performed using the previously  
156 outlined methodology (Kourentas et al., 2018). Briefly, the gastric volume was initially filled with 250  
157 mL of Level II FaSSGF in a 500 mL capacity mini vessel (Erweka). The duodenal compartment was  
158 initially filled with 40 mL of Level II FaSSIF in a mini vessel with 100 mL capacity from Distek (NJ,  
159 USA). The stirring speed was set at 75 rpm in both compartments. Experiments are performed at  
160 37°C for 45 min using a three-channel peristaltic pump (Reglo ICC pump, part ISM 4308, Ismatec,  
161 Wertheim, Germany). To replicate GI transfer, media was pumped from the gastric compartment  
162 into the duodenal compartment (flow rate = F1), with media flowing out of the duodenal  
163 compartment to replicate the transfer of both undissolved and unabsorbed drug to the lower  
164 regions of the small intestine (flow rate = F). To maintain both the volume and composition of the  
165 fluid in the duodenal compartment throughout the experiment, media from the reservoir  
166 compartment was pumped into the duodenal compartment at a flow rate (F2), such that the total  
167 flow into the duodenal compartment is identical to flow out of the duodenal compartment ( $F = F1 +$   
168  $F2$ ). The reservoir compartment consisted of a series of phosphate buffer solutions containing  
169 sodium chloride, sodium taurocholate, and phosphatidylcholine to keep the composition of  
170 simulated duodenal contents constant during the experiment (Kourentas et al., 2018, 2016). Flow  
171 rates are changed every 10 min and sampling was performed at the midpoint of these ten-minute

172 intervals, so that emptying of the gastric compartment follows apparent first order kinetics, with a  
173 half-life of 15 minutes. Upon collection, each sample from the duodenal compartment was split into  
174 two parts:

- 175 • The first part was immediately filtered through 0.45 µm regenerated cellulose filters (Titan  
176 3, 17 mm). This filtrate was then divided into two portions. The first portion was used to  
177 determine the dissolved concentration of drug in the duodenal compartment. The second  
178 portion of the filtrate was used to estimate the equilibrium solubility of the drug in the  
179 medium, by incubating it (37°C, 75 oscillations/min) in the presence of an excess of solid  
180 compound until equilibrium was reached.
- 181 • The second part was used to determine the total presence of drug (dissolved and solid drug)  
182 in the duodenal compartment. This part is immediately diluted with the mobile phase  
183 (without filtration), with the total drug concentration quantified using HPLC, with the HPLC  
184 method outlined in section 2.2.6.

185 In this study, only experiments with Cataflam® and Voltfast® were performed; BioGIT data for  
186 Norvir® have recently been published (Van Den Abeele et al., 2020).

#### 187 2.2.6. Assay methods

188 Small-scale two-stage biphasic and D-P systems: Drug content was quantified primarily using *in situ*  
189 fibre optic UV probes. Different standard spectra were collected for the neutral and ionised forms of  
190 each compound with the detection wavelengths shown in the supplementary material (Table S3). An  
191 excipient in the ritonavir ASD formulation caused significant turbidity in the aqueous media, leading  
192 to a high degree of scattering in the UV spectra recorded from the aqueous layer and donor  
193 compartments from the small-scale two-stage biphasic and D-P systems, respectively. Due to this  
194 scattering present for the ritonavir ASD formulation, it was not possible to quantify drug in these  
195 compartments using *in situ* UV probes. However, the decanol layer and acceptor chamber spectra  
196 were unaffected by this scattering.

197 As aqueous concentration data from the small-scale two-stage biphasic system experiment were  
198 used to calculate a precipitation rate constant for the PBB model constructed to reflect normal  
199 gastric acid rate secretions, offline ultra-performance liquid chromatography (UPLC) quantification  
200 methods were used to quantify ritonavir concentrations in the aqueous phase during the  
201 experiments performed under conditions assuming normal gastric acid rate conditions. Therefore,  
202 samples taken from aqueous layer using the automated liquid handling needle during the first 90  
203 min from the ritonavir biphasic experiments were quantified offline using an Acquity UPLC H-Class  
204 Plus (Waters Corporation, MA, USA) with BEH C18 (1.7  $\mu\text{m}$  2.1  $\times$  50 mm) column using a PDA  
205 detector, FTN-H sample manager and a quaternary solvent manager. Data was collected and  
206 processed using Empower 3 software (Waters Corporation). The mobile phase comprised a mixture  
207 of acetonitrile and 0.1 % formic acid (v/v) using a gradient, with further information provided in the  
208 supplementary materials (Table S4). The injection volume was 5  $\mu\text{L}$  with a detection wavelength of  
209 254 nm and the limit of quantitation (LOQ) was 0.3  $\mu\text{g}/\text{mL}$ .

210 Erweka mini-paddle apparatus and BioGIT system: Diclofenac samples were quantified using a  
211 Dionex UltiMate 3000 HPLC system (Thermo Scientific Inc., MA, USA), with data collected and  
212 processed using Chromeleon software (Thermo Scientific Inc.). The mobile phase for diclofenac was  
213 ammonium formate pH 3.5 (10 mM): methanol, 25:75 (v/v) with a detection wavelength of 279 nm  
214 and LOQ of 0.3  $\mu\text{g}/\text{mL}$ . Ritonavir samples were quantified using a Spectra HPLC system consisting of  
215 a P1000 pump, an AS1000 autosampler, a UV2000 detector, and an SN4000 controller which was  
216 controlled by the Chromquest® software (version 2.51, Thermo Scientific Inc.). The mobile phase for  
217 ritonavir consisted of 0.25 % Phosphoric acid: acetonitrile, 45:55 (v/v) and the detection wavelength  
218 was 240 nm with a LOQ of 1  $\mu\text{g}/\text{mL}$ . Analysis of both drug substances used a Fortis C18 column (3  
219  $\mu\text{m}$ , 150  $\times$  3 mm), a flow rate of 0.5 mL/min and an injection volume was 50  $\mu\text{L}$ .

220           2.2.7. Physiologically based biopharmaceutics modelling

221 PBB modelling was carried out using the ADAM model which is available as part of the Simcyp

222 simulator (Version 18, Release 2, Certara UK Limited, Sheffield, UK) with the parameters for

223 diclofenac and ritonavir, shown in Table 1 and Table 2, respectively. Ten virtual trials using the same

224 number of subjects as the respective clinical studies were simulated in each case and were

225 conducted using the Sim-Healthy Volunteers population in the Simcyp software.

226 Diclofenac PBB modelling was completed using the stepwise workflow *IVIV\_E (In Vitro In Vivo*

227 *Extrapolation)* of solubility and dissolution (Pathak et al., 2019, 2017). Solubility values were

228 estimated using literature data (Guhmann et al., 2013). The diffusion layer model (DLM) scalar was

229 used as part of the dissolution model in the simulator, with the value estimated using the SIVA

230 (Simcyp In Vitro Analysis) software from the dissolution profiles obtained from the Erweka mini-

231 paddle apparatus. A sensitivity analysis was conducted to evaluate the effect of precipitation, if any,

232 on the modelled plasma profile. The transit times of the drug through the GI tract were set at the

233 default mean residence times in the simulator, with a first order gastric emptying process (Hens et

234 al., 2018; Jamei et al., 2009). The distribution of diclofenac was estimated using intravenous (IV) data

235 (Hinz et al., 2005; Willis et al., 1979) and adjusted using the volume of distribution (Davies and

236 Anderson, 1997), via the tissue-plasma partition coefficient ( $K_p$ ) scalar. Elimination was estimated

237 from IV data (Hinz et al., 2005; Willis et al., 1979).

238 The biorelevant solubility values were directly inputted into the models for the ritonavir ASD,

239 bypassing the requirement to estimate the micellar: buffer partition coefficients in SIVA. Identifying

240 an appropriate solubility value is challenging for enabling formulations (Litou et al., 2020, 2019). The

241 plateau values from the Erweka mini-paddle apparatus experiments were taken to represent the

242 ‘effective’ solubility of the formulated drug. The DLM scalar was used as part of the dissolution

243 model, with the value estimated using the SIVA software from the dissolution profiles obtained from

244 the Erweka mini-paddle apparatus. While it is feasible to use small-scale single stage dissolution

245 experiments in the inForm or  $\mu$ Diss platforms to model dissolution, in this instance the data was  
246 already available from the Erweka mini-paddle apparatus. Dissolution in the model occurs in the  
247 stomach and the intestine of any solid drug, regardless of whether it is undissolved or precipitated  
248 drug. An empirical first-order precipitation rate constant (PRC) was estimated by fitting aqueous  
249 concentration profiles from the small-scale two-stage biphasic system experiments using Microsoft  
250 Excel tools (supplementary materials, Figure S1), as previously outlined (O'Dwyer et al., 2020).  
251 Precipitation was considered to have terminated when the drug concentration in the aqueous layer  
252 plateaued. Ritonavir was modelled to precipitate to its amorphous state based on previous pH shift  
253 dissolution experiments (Miller et al., 2016; Xu et al., 2017). Previous experiments indicated that  
254 PRCs estimated from the small-scale two-stage biphasic system were better than those estimated  
255 from small-scale two-stage D-P experiments (O'Dwyer et al., 2020). Therefore, the small-scale two-  
256 stage D-P system results were not used to estimate precipitation in the PBB model. To simulate  
257 hypochlorhydria, the fasted stomach pH in the model was increased to 5.0, with a DLM scalar under  
258 hypochlorhydric conditions (Segregur et al., 2021) estimated in the SIVA tool from the  
259 hypochlorhydric dissolution profiles obtained from the Erweka mini-paddle apparatus. The transit  
260 times of the drug through the GI tract were set at the default mean residence times in the simulator,  
261 with a first order gastric emptying process (Hens et al., 2018; Jamei et al., 2009). The volume of  
262 distribution was estimated using the physicochemical properties of the molecule, with a Kp scalar  
263 employed to adjust the volume of distribution. Elimination parameters were modelled using enzyme  
264 kinetic studies (Koudriakova et al., 1998) using information provided as part of the "SV-Ritonavir"  
265 compound default file in the simulator.

266 The Fold Difference (FD) ratio of the predicted vs. observed parameters, i.e., area under the plasma  
267 concentration-time curve (AUC), maximum plasma concentration ( $C_{max}$ ), and time to reach  $C_{max}$  ( $T_{max}$ )  
268 were used to evaluate the modelled results. In addition, the absolute average fold error (AAFE)  
269 (equation 1) was calculated (Andreas et al., 2017; Poulin and Theil, 2009) to evaluate the modelled  
270 mean plasma profiles.  $n$  is the number of time points at which the concentration was determined,

271 with *predicted i* and *observed i* being the predicted and observed concentrations at a given time  
272 point *i*. AAFE shows the absolute error of the simulation compared to the observed profiles, with  
273 values of < 2 considered to show a successful simulation.

274

$$AAFE = 10^{\left(\frac{1}{n}\right) * \sum |Log\left(\frac{predicted\ i}{observed\ i}\right)|} \quad (1)$$

275

276 2.2.8. Extraction of published *in vivo* data

277 Previously published *in vivo* data for diclofenac (Marzo et al., 2000; Van Den Abeele et al., 2017) and  
278 ritonavir (Ng et al., 2008; Van Den Abeele et al., 2020) were extracted using WebPlotDigitizer  
279 (version 4.2, WebPlotDigitizer, CA, USA).

280

## 281 3. Results and Discussion

### 282 3.1. Diclofenac

#### 283 3.1.1. Small-scale two-stage biphasic system

284 Initially both formulations appeared to be transiently highly supersaturated in the gastric sector,  
285 before precipitation of both formulations was subsequently observed (Figure 1). Despite this  
286 precipitation, the powder formulation had a higher concentration of diclofenac in solution compared  
287 to the tablet formulation at the end of the testing period in the gastric sector; mean  $\pm$  SD (n = 3)  
288 values were  $8.48 \pm 0.43$  and  $2.03 \pm 0.21$  % (w/w) of the dose for the powder and the tablet  
289 formulation, respectively. In particular, the powder formulation appeared to be supersaturated  
290 compared to the equilibrium concentration of the free acid in dilute HCl (Guhmann et al., 2013) of  
291 approx. 1.3 % (converted to an equivalent percentage (w/w) of the dose), indicating a solubilising  
292 effect of the formulation's excipients (Wisdom Pharmaceutical Technology Co Limited, 2020).  
293 However, an in-depth study of the solubilising effect of each excipient in the formulation was  
294 beyond the scope of this work.

295 Upon the switch to intestinal conditions, the drug substance from both formulations was rapidly  
296 dissolved in the aqueous layer and the drug readily partitioned into the decanol layer. Interestingly,  
297 the ionisation of diclofenac in the intestinal sector did not prevent partitioning into the decanol  
298 layer, with more than 85 % (w/w) of the dose in solution in the decanol layer for both formulations  
299 at the end of the experiment. The results from both layers indicated that both formulations would  
300 dissolve rapidly upon entry into the upper small intestine and that a similar AUC should be achieved  
301 by both formulations, correlating with the observed  $AUC_{0-\infty}$  from the clinical study (Marzo et al.,  
302 2000). However, the more rapid  $C_{max}$  and greater  $AUC_{0-2h}$  observed for the powder formulation in  
303 the clinical study was not highlighted by the small-scale two-stage biphasic system results, with  
304 similar concentration-time profiles recorded for both formulations using the setup (Figure 1).

305 3.1.2. Small scale two-stage D-P system

306 Similar to the small-scale two-stage biphasic system experiments, both formulations were initially  
307 highly supersaturated in the gastric sector in the donor chamber with the greatest mean  $\pm$  SD (n = 3)  
308 values measured concentration in the gastric sector of  $13.88 \pm 0.98$  and  $6.27 \pm 1.10$   $\mu\text{g/mL}$  for the  
309 powder and the tablet formulation, respectively, compared to the reported solubility of  $2.49$   $\mu\text{g/mL}$   
310 in dilute HCl (Guhmann et al., 2013). Precipitation of both formulations subsequently occurred in the  
311 donor chamber during the gastric sector (Figure 2a). At the end of the gastric sector, the  
312 concentration of the powder formulation was higher than the tablet formulation in the donor  
313 chamber; mean  $\pm$  SD (n = 3) values were  $4.25 \pm 0.80$  and  $1.08 \pm 0.13$  % (w/w) of the dose for powder  
314 and tablet formulation, respectively. The powder formulation appeared to be supersaturated  
315 compared to the equilibrium concentration of the free acid in dilute HCl (Guhmann et al., 2013) of  
316 approx. 1.1 % (converted to an equivalent percentage (w/w) of the dose). While these  
317 concentrations in donor chamber at the end of the gastric sector are lower than the equivalent  
318 concentrations in the small-scale two-stage biphasic system, the membrane in the small scale two-  
319 stage D-P system is *in situ* throughout the experiment allowing 'absorption' of drug into the acceptor  
320 chamber during the gastric sector, unlike the small-scale two-stage biphasic system.

321 Upon transition to intestinal conditions, the donor chamber concentrations indicated that both  
322 formulations would rapidly dissolve. The powder formulation was more rapidly dissolved compared  
323 to the tablet formulation, correlating with the more rapid  $C_{\text{max}}$  observed for the powder formulation  
324 in the clinical study (Marzo et al., 2000), unlike the small-scale two-stage biphasic system  
325 experiments which showed a minimal difference between formulations (Figure 1).

326 The concentration in the acceptor chamber for the tablet (Figure 2b) was lower than the powder  
327 formulation throughout the experiment, with mean  $\pm$  SD (n = 3) values at the end of the experiment  
328 of  $3.33 \pm 0.53$  and  $5.25 \pm 0.50$  % (w/w) of the dose for the tablet and powder formulation,  
329 respectively. Most of the difference in acceptor chamber concentrations between formulations (1.16

330 % (w/w) of the dose) was due to flux of drug into the acceptor chamber during the gastric sector.  
331 The predominantly nonionised drug could readily pass through the membrane during the gastric  
332 sector, as the membrane was *in situ* throughout the experiment. This feature of the setup could be  
333 useful to simulate possible gastric absorption, if any, which may partly account for the greater  $C_{max}$   
334 observed for the powder formulation. While this is some evidence for gastric absorption of  
335 diclofenac in rats (Rubbens et al., 2018) and humans (Vidon et al., 1989), this discussion regarding  
336 the significance of gastric absorption is highly contentious and beyond the scope of this study.  
337 A disadvantage of both small-scale systems is that any variance due to differences in gastric  
338 emptying times between the formulations cannot be detected, as the switch from gastric to  
339 intestinal conditions occurs at a single time point in both systems. Another disadvantage of using  
340 small-scale methods is the requirement to crush the dosage form to scale-down the dose. While the  
341 rupture time of the gelatin capsules will somewhat replicate the disintegration time of the tablet,  
342 the effect of disintegration as differentiator between the formulations is overlooked.

### 343 3.1.3. Erweka mini-paddle apparatus

344 In Level III FaSSGF, both formulations supersaturated in the dissolution medium for a few minutes,  
345 followed by precipitation of the free acid down to the equilibrium solubility (Figure 3a) (Guhmann et  
346 al., 2013). Rapid and complete (> 95 %) diclofenac dissolution from both formulations was observed  
347 in Level II biorelevant intestinal media (Figure 3b). The effect of disintegration on the formulations  
348 was clearly observed with a delayed release of drug from the tablet formulation. In contrast,  
349 dissolution from the powder formulation was very rapid with > 95 % of the dose in solution by the  
350 first time point after 5 minutes (Figure 3b).

### 351 3.1.4. BioGIT system

352 The tablet formulation had a 14.5 % smaller  $AUC_{Duodenal, 0-0.75h}$  compared to the powder formulation  
353 (33.50 vs. 39.19  $\mu\text{g. h/mL}$ ,  $n = 3$ ) using the BioGIT system (Figure 4). For both formulations, no solid  
354 drug was detected in the intestinal chamber, due to the high solubility of diclofenac in an intestinal

355 environment. This matched behaviour observed in the duodenal aspirates of healthy volunteers,  
356 after administration of the tablet formulation in the fasting state (Van Den Abeele et al., 2017,  
357 2016). Unfortunately, intraluminal concentrations after administration of the powder formulation  
358 are not available.

359 The clinical study in healthy adults has shown that the tablet formulation had a 35 % smaller  
360  $AUC_{Systemic, 0-2h}$  than the powder formulation (Marzo et al., 2000), with the powder formulation also  
361 having an earlier median  $t_{max}$  than the tablet formulation (0.25 vs. 0.63 h). This difference in early  
362 exposure between the formulations was successfully simulated by the BioGIT system data on a  
363 qualitative basis; the mean  $AUC_{Duodenal, 0-0.75h}$  value estimated from concentration vs. time BioGIT  
364 system data for the tablet formulation was lower than the corresponding value for the powder  
365 formulation. Although BioGIT system has not been designed to capture physiological differences in  
366 gastric emptying rates between formulations, especially when the *in vivo* data are highly variable as  
367 evidenced from the gastric and duodenal aspirate samples (Van Den Abeele et al., 2017, 2016),  
368 BioGIT system diclofenac data collected in this study may contribute to understanding the  
369 relationship of BioGIT system data with human data on a quantitative basis (Kourentas et al., 2018).

### 370 3.1.5. Physiologically based biopharmaceutics modelling

371 PBB modelling for the tablet formulation using the DLM scalar and disintegration parameters, both  
372 estimated from the Erweka mini-paddle apparatus data, resulted in a good fit (AAFE = 1.55) relative  
373 to the previously observed average plasma profile in adults (Figure 5a, Table 3). The simulated  
374 duodenal concentrations showed complete dissolution of the tablet formulation in the model,  
375 analogous to the BioGIT system data. The modelled duodenal concentrations for both diclofenac  
376 formulations are in-line with the concentrations in the BioGIT duodenal compartment (Figure 4).

377 As the powder for oral solution is pre-dissolved in a glass of water prior to administration, it was  
378 treated as an oral solution in the model. This model for the powder formulation indicated that the  
379 key parameters for modelling the rate of oral absorption for diclofenac were the gastric residence

380 time in the simulated population and the permeability of drug in the upper small intestine. In an  
381 attempt to replicate this rapid early exposure of the powder formulation, the mean residence time  
382 in the stomach was reduced from the default of 0.36 to 0.05 h. Despite this reduced gastric  
383 residence time, the modelled  $T_{max}$  was later with a smaller  $C_{max}$  compared to the clinical results  
384 (Figure 5b, Table 3), which indicated that permeability in the upper small intestine was  
385 underestimated in the model. A sensitivity analysis was carried out examining the effect of intestinal  
386 permeability on the simulated plasma profile in the model, showing an earlier  $T_{max}$  and increased  
387  $C_{max}$  with increasing intestinal permeability values (Supplementary Material, Figure S2).

388 While it is unlikely that intestinal permeability varied significantly between the formulations, it  
389 appears the rate limiting step of drug absorption was different between the formulations. The  
390 absorption of drug from the tablet appeared to be delayed due to disintegration, while absorption of  
391 drug from the powder for oral solution was primarily dependent on gastric emptying and/or the  
392 intestinal permeability of the drug. For both formulations, the models were not sensitive to  
393 precipitation in the stomach as any solid drug was rapidly dissolved in the intestine, due to its high  
394 solubility in intestinal conditions.

### 395 *3.2. Ritonavir*

#### 396 3.2.1. Small-scale two-stage biphasic system

397 Rapid precipitation of the drug was observed upon transfer from gastric to intestinal conditions in  
398 the experiment simulating normal gastric conditions (Figure 6). The precipitation rate constant  
399 calculated from this experiment was incorporated into a PBB model, as outlined in section 2.2.7.  
400 Similar concentrations were observed in the decanol layer using both normal and hypochlorhydric  
401 gastric conditions. This correlates nicely with the information provided in the summary of product  
402 characteristics (SmPC), which indicates that concurrent administration of a proton pump inhibitor  
403 (PPI) or  $H_2$  antagonist did not affect the efficacy of ritonavir, with only a small decrease in drug  
404 exposure (AbbVie Deutschland GmbH & Co. KG., 2016). In addition, duodenal aspirates from fasted

405 healthy volunteers showed no significant change in ritonavir concentration after administration with  
406 esomeprazole (Van Den Abeele et al., 2020). As the small-scale two-stage biphasic system only  
407 accounts for the changes in gastric pH caused by the PPI, it does not simulate any other physiological  
408 effects caused by the PPI which may affect systemic concentrations (Babaei et al., 2009; de Waal et  
409 al., 2020; Segregur et al., 2019; Van Den Abeele et al., 2020).

#### 410 3.2.2. Small-scale two-stage D-P system

411 Profiles in the acceptor compartment suggest no significant impact of hypochlorhydric conditions to  
412 the absorption of ritonavir from the ASD product (Figure 7), in-line with the *in vivo* observations  
413 (AbbVie Deutschland GmbH & Co. KG., 2016; Morcos et al., 2014; Van Den Abeele et al., 2020).  
414 Analogous to the small-scale two-stage biphasic system experiments, this hypochlorhydric setup  
415 only accounts for changes in the gastric pH caused by the PPI.

#### 416 3.2.3. Erweka mini-paddle apparatus

417 Using the Erweka mini-paddle apparatus, there was a higher percentage of the dose in solution in  
418 Level III FaSSGF at a normal gastric pH compared to the hypochlorhydric conditions; mean  $\pm$  SD (n =  
419 3) values were  $67.59 \pm 1.76$  and  $7.67 \pm 0.06$  % (w/w) of the dose under normal and reduced gastric  
420 acid conditions, respectively (Figure 8). However, the clinical study showed that concentrations of  
421 drug in the duodenum were not significantly affected by the hypochlorhydric gastric conditions  
422 (AbbVie Deutschland GmbH & Co. KG., 2016; Morcos et al., 2014; Van Den Abeele et al., 2020).  
423 These results highlighted the necessity to incorporate the GI transfer process as part of the *in vitro*  
424 testing, to improve the understanding of the behaviour of this ritonavir ASD. Dissolution data from  
425 the Erweka mini-paddle apparatus experiments were incorporated into an PBB model and are  
426 discussed in parallel with the data from the small-scale two-stage biphasic system in section 3.2.4.

#### 427 3.2.4. Physiologically based biopharmaceutics modelling

428 Initially, modelling was completed using the default DLM scalar (i.e., DLM = 1) without incorporating  
429 precipitation to establish if a decent model could be established without including experimentally

430 derived values for either precipitation or dissolution in the model. This model produced a poor fit  
431 relative to the *in vivo* profile (AAFE = 3.52), with a very large overestimation of both AUC and  $C_{max}$   
432 (Table 4). This highlighted that experimentally determined values for the dynamic dissolution  
433 process are vital to incorporate into the model. Therefore, the impact of the dynamic dissolution  
434 process, incorporating dissolution and precipitation of drug (McAllister, 2010), on the oral  
435 absorption of ritonavir from Norvir® was investigated.

436 The effects of including experimentally determined values for dissolution and precipitation were first  
437 examined individually in the model to improve the understanding of the sensitivity of the  
438 parameters in the model. Thus, the dissolution results from the Erweka mini-paddle apparatus  
439 dissolution results simulating both gastric and intestinal conditions (section 3.2.3) were included in  
440 the model without precipitation present. The dissolution rate was incorporated into the model via  
441 the DLM scalar, estimated in SIVA from the Erweka mini-paddle apparatus dissolution results. This  
442 model resulted in an overestimation of both  $C_{max}$  and AUC (Figure 9, Table 4, AAFE 1.50), highlighting  
443 that slow and/or incomplete dissolution was not the sole limiting factor for the oral absorption of  
444 the ritonavir from Norvir®.

445 The effect of precipitation on oral absorption was then examined. Previous studies have shown that  
446 the small-scale two-stage biphasic system was a suitable *in vitro* method to calculate the PRC of a  
447 weakly basic drug, as it transitions from gastric to intestinal conditions (O'Dwyer et al., 2020). Using  
448 the biphasic results, a high PRC was calculated of  $9.45 \text{ h}^{-1}$  indicating a very rapid precipitation of drug  
449 upon entry into the intestine. The critical supersaturation ratio (CSR) was 1, as the critical  
450 supersaturation concentration determined from solvent shift experiments of ritonavir using Level II  
451 intestinal media ( $35.96 \mu\text{g/mL}$ ) was below the observed kinetic solubility of ritonavir from Norvir® in  
452 Level II intestinal media (Xu et al., 2017). This effect was potentially due to the sorbitan laurate in  
453 the formulation (AbbVie Deutschland GmbH & Co. KG., 2016), which is believed to alter the  
454 precipitation and crystallisation behaviour of drugs (Chen et al., 2017).

455 Simulations using the PRC calculated from the small-scale two-stage biphasic system experiments  
456 were carried out employing the default DLM scalar value (i.e., DLM = 1) in the model, to examine  
457 whether precipitation alone was the key limiting factor for the oral absorption of the ritonavir ASD  
458 formulation. Modelling using the default DLM scalar resulted in an overestimation of the AUC and  
459  $C_{max}$  compared to the clinical results (Figure 9, Table 4, AAFE 1.37), indicating that precipitation alone  
460 did not fully account as the limiting factor for drug absorption. Therefore, the effect of dissolution  
461 and precipitation together on oral absorption was examined.

462 Using DLM scalar values and a precipitation rate estimated from the Erweka mini-paddle apparatus  
463 and the small-scale two-stage biphasic system experiments, respectively, improved the performance  
464 of the model relative to the previously published plasma data in adults (Figure 9). The modelled AUC  
465 and  $C_{max}$  using the 'combined' model had a smaller prediction error (PE) relative to the *in vivo* results  
466 compared to the other modelled profiles (Table 4) with the smallest AAFE of 1.26. Therefore, both  
467 dissolution and precipitation parameters were necessary for building an adequate model for  
468 Norvir®. While keeping in mind any limitations or uncertainties regarding modelling, this highlights  
469 the benefit of combining PBB modelling with biorelevant *in vitro* testing as part of the drug  
470 formulation development process, even after clinical testing, as modelling can be a source of  
471 additional valuable insight. In this study, the modelling after the clinical study improved the  
472 understanding of the factors limiting oral absorption which were not directly apparent from the  
473 clinical study results alone. Furthermore, the modelled duodenal concentrations under normal  
474 gastric conditions are in-line with the concentrations in the BioGIT duodenal compartment (Van Den  
475 Abeele et al., 2020) (Figure 10a).

476 The model under hypochlorhydric conditions in the stomach, resulted in a minor decrease in the  
477 AUC and  $C_{max}$  (Table 4), in-line with the range provided in the summary of product characteristics (6  
478 – 18 %) for Norvir (AbbVie Deutschland GmbH & Co. KG., 2016) and results from a clinical study (n =  
479 13), where the effects of co-administration of ranitidine or omeprazole on the pharmacokinetics of

480 danoprevir/ritonavir were examined (Morcos et al., 2014). While the modelled duodenal  
481 concentrations under hypochlorhydric conditions appear to be lower than the concentrations BioGIT  
482 duodenal compartment (Van Den Abeele et al., 2020) (Figure 10b), early duodenal exposure in the  
483 initial 45 min is unlikely to be the critical factor in ritonavir absorption considering the reported  $C_{max}$   
484 and half-life of ritonavir of 3.2 and 5.5 hr, respectively (Ng et al., 2008). Plasma profiles from the Van  
485 den Abeele *et al.* study examining the effect of pre-treatment with a PPI were inconclusive, due to  
486 the extremely large variability observed between the healthy volunteers, potentially related to the  
487 small number of participated volunteers (n = 5) (Van Den Abeele et al., 2020). In addition, the  
488 authors deduced that physiological effects of the PPI other than the impact on gastric pH, such as a  
489 change in GI fluid volumes (Segregur et al., 2019), may have impacted the systemic plasma profiles  
490 (de Waal et al., 2020; Van Den Abeele et al., 2020). The choice of PPI selected for co-administration  
491 with ritonavir may be a significant factor with less pronounced effects on gastric volumes associated  
492 with omeprazole compared to other PPIs (Gursoy et al., 2008). As the PBB model presented in this  
493 study only simulated the effect on the gastric pH caused by the PPI, it would overlook any of these  
494 potential physiological effects of the PPI. With further understanding of the complete physiological  
495 effects of the PPIs, improved PBB models could be designed to predict the effect of PPI pre-  
496 treatment.

497

498

#### 499 4. Concluding Remarks

500 This study indicates that selection of the appropriate *in vitro* method for evaluating the intraluminal  
501 performance of poorly soluble, ionisable drugs depends primarily on the characteristics of the drug  
502 substance.

503 For the diclofenac potassium formulations, the Erweka mini-paddle apparatus results in Level II  
504 biorelevant media alone were sufficient to capture the effects, if any, on *in vivo* dissolution. For  
505 drugs such as diclofenac, the issue of availability and ease of operation of the *in vitro* system are the  
506 key points of consideration.

507 For Norvir®, detailed information on its behaviour both under gastric simulated conditions and  
508 under conditions simulating those in the upper small intestine was crucial for understanding the  
509 luminal performance. An improved PBB model was created by incorporating both dissolution and  
510 precipitation parameters into the model using results from both the Erweka mini-paddle apparatus  
511 and the small-scale two-stage biphasic system experiments, respectively. Simulation of the  
512 gastrointestinal transfer process from the stomach to the small intestine was necessary to evaluate  
513 the effects of hypochlorhydric conditions on the luminal performance of the ritonavir ASD.

514 Using *in situ* UV dip probes to quantify drug in both small-scale setups facilitated a rapid throughput  
515 of experiments, by avoiding off-line quantitation steps. The advantage of small-scale two-stage  
516 biphasic system was the more rapid absorption of drug in the intestinal conditions compared to the  
517 small-scale two-stage D-P system. In addition, the small-scale two-stage biphasic system allowed the  
518 flexibility to introduce the absorption sink as determined by the user, whereas the absorption sink is  
519 in place throughout the small-scale two-stage D-P system experiments. On the other hand, the setup  
520 of the small-scale two-stage D-P system platform allowed the triplicate experiments to be in parallel,  
521 facilitating a more rapid throughput than the small-scale two-stage biphasic system. Furthermore,  
522 the small-scale two-stage D-P system experiments have a smaller operating volume (20 mL) than the  
523 small-scale two-stage biphasic system (40 mL), allowing for a reduced quantity of drug employed in

524 these experiments. The Erweka mini-paddle apparatus experiments are less complex to operate  
525 than the BioGIT system and can be run in parallel. However, the BioGIT system is useful to provide  
526 information about the dynamic behaviour of the drug in the duodenum.

527 Regardless of the type of the drug substances, early in the drug development process, when  
528 availability of drug amounts and/or dose units is limited, the Erweka mini-paddle apparatus or the  
529 BioGIT system [at least if not at its mini-version  
530 (<https://pergamos.lib.uoa.gr/uoa/dl/object/2775881>)] may not be applicable. Therefore, small-scale  
531 systems are necessary at this stage. This study examined the application of the small-scale systems  
532 to comparatively assess performance of formulations in the GI tract and to obtain parameters for  
533 PBB modelling. However, other applications of these small-scale systems are potentially possible,  
534 such as directly obtaining a quantitative estimation of oral absorption in early development, and are  
535 worthy of further investigation in future studies. When applying small-scale setups, it is important to  
536 be mindful of limitations associated with the respective setups, such as the necessity to crush the  
537 dosage forms, when interpreting the data. At later stages of development, full-scale methods should  
538 be employed.

## 539 Acknowledgments

540 This work was supported by the European Union's Horizon 2020 Research and Innovation  
541 Programme under grant agreement No 674909 (PEARRL).

## 542 References

- 543 AbbVie Deutschland GmbH & Co. KG., 2016. Norvir 100mg tablets. Summary of Product  
544 Characteristics.
- 545 Accord-UK Ltd, 2018. Diclofenac Potassium 50 mg Tablets. Summary of Product Characteristics.
- 546 Andreas, C.J., Pepin, X., Markopoulos, C., Vertzoni, M., Reppas, C., Dressman, J.B., 2017. European  
547 Journal of Pharmaceutical Sciences Mechanistic investigation of the negative food effect of  
548 modified release zolpidem. *Eur. J. Pharm. Sci.* 102, 284–298.  
549 <https://doi.org/10.1016/j.ejps.2017.03.011>
- 550 Babaei, A., Bhargava, V., Aalam, S., Scadeng, M., Mittal, R.K., 2009. Effect of proton pump inhibition  
551 on the gastric volume: Assessed by magnetic resonance imaging. *Aliment. Pharmacol. Ther.* 29,  
552 863–870. <https://doi.org/10.1111/j.1365-2036.2009.03947.x>
- 553 Bou-Chacra, N., Melo, K.J.C., Morales, I.A.C., Stippler, E.S., Kesisoglou, F., Yazdanian, M., Löbenberg,  
554 R., 2017. Evolution of Choice of Solubility and Dissolution Media After Two Decades of  
555 Biopharmaceutical Classification System. *AAPS J.* 19, 989–1001.  
556 <https://doi.org/10.1208/s12248-017-0085-5>
- 557 Brouwers, J., Brewster, M.E., Augustijns, P., 2009. Supersaturating drug delivery systems: The  
558 answer to solubility-limited oral bioavailability? *J. Pharm. Sci.* 98, 2549–2572.  
559 <https://doi.org/10.1002/jps.21650>
- 560 Brouwers, J., Geboers, S., Mols, R., Tack, J., Augustijns, P., 2017. Gastrointestinal behavior of  
561 itraconazole in humans – Part 1: Supersaturation from a solid dispersion and a cyclodextrin-  
562 based solution. *Int. J. Pharm.* 525, 211–217.  
563 <https://doi.org/https://doi.org/10.1016/j.ijpharm.2017.04.029>
- 564 Chen, B., Zhu, L., Zhang, F., Qiu, Y., 2017. Chapter 31 - Process Development and Scale-Up: Twin-  
565 Screw Extrusion, in: Qiu, Yihong, Chen, Y., Zhang, G.G.Z., Yu, L., Mantri, R. V (Eds.), *Developing*  
566 *Solid Oral Dosage Forms (Second Edition)*. Academic Press, Boston, pp. 821–868.  
567 <https://doi.org/https://doi.org/10.1016/B978-0-12-802447-8.00031-5>
- 568 Chuasuwan, B., Binjesoh, V., Polli, J.E., Zhang, H., Amidon, G.L., Junginger, H.E., Midha, K.K., Shah,  
569 V.P., Stavchansky, S., Dressman, J.B., Barends, D.M., 2009. Biowaiver monographs for  
570 immediate release solid oral dosage forms: Diclofenac sodium and diclofenac potassium. *J.*  
571 *Pharm. Sci.* 98, 1206–1219. <https://doi.org/10.1002/jps.21525>
- 572 Davies, N.M., Anderson, K.E., 1997. Clinical Pharmacokinetics of Diclofenac Therapeutic Insights and  
573 Pitfalls. *Clin. Pharmacokinet.* 33, 184–213.
- 574 de Waal, T., Rubbens, J., Grimm, M., Vandecaveye, V., Tack, J., Weitschies, W., Brouwers, J.,  
575 Augustijns, P., 2020. Exploring the Effect of Esomeprazole on Gastric and Duodenal Fluid  
576 Volumes and Absorption of Ritonavir. *Pharmaceutics* 12, 670.  
577 <https://doi.org/10.3390/pharmaceutics12070670>
- 578 Denissen, J.F., Grabowski, B.A., Johnson, M.K., Buko, A.M., Kempf, D.J., Thomas, S.B., Surber, B.W.,  
579 1997. Metabolism And Disposition of the HIV-1 Protease Inhibitor Ritonavir (ABT-538) in Rats,  
580 Dogs, and Humans. *Drug Metab. Dispos.* 25, 489.
- 581 Guhmann, M., Thommes, M., Gerber, F., Pöllinger, N., Klein, S., Breitzkreutz, J., Weitschies, W., 2013.  
582 Design of biorelevant test setups for the prediction of diclofenac in vivo features after oral  
583 administration. *Pharm. Res.* 30, 1483–1501. <https://doi.org/10.1007/s11095-013-0974-y>
- 584 Gursoy, O., Memiş, D., Sut, N., 2008. Effect of proton pump inhibitors on gastric juice volume, gastric

585 pH and gastric intramucosal pH in critically ill patients: A randomized, double-blind, placebo-  
586 controlled study. *Clin. Drug Investig.* 28, 777–782. [https://doi.org/10.2165/0044011-](https://doi.org/10.2165/0044011-200828120-00005)  
587 200828120-00005

588 Hens, B., Brouwers, J., Corsetti, M., Augustijns, P., 2016. Supersaturation and Precipitation of  
589 Posaconazole Upon Entry in the Upper Small Intestine in Humans. *J. Pharm. Sci.* 105, 2677–  
590 2684. <https://doi.org/10.1002/jps.24690>

591 Hens, B., Talattof, A., Paixão, P., Bermejo, M., Tsume, Y., Löbenberg, R., Amidon, G.L., 2018.  
592 Measuring the Impact of Gastrointestinal Variables on the Systemic Outcome of Two  
593 Suspensions of Posaconazole by a PBPK Model. *AAPS J.* 20, 57. [https://doi.org/10.1208/s12248-](https://doi.org/10.1208/s12248-018-0217-6)  
594 018-0217-6

595 Hinz, B., Chevts, J., Renner, B., Wuttke, H., Rau, T., Schmidt, A., Szelenyi, I., Brune, K., Werner, U.,  
596 2005. Bioavailability of diclofenac potassium at low doses. *Br. J. Clin. Pharmacol.* 59, 80–84.  
597 <https://doi.org/10.1111/j.1365-2125.2005.02226.x>

598 Hsu, A., Granneman, G.R., Bertz, R.J., Laboratories, A., Park, A., 1998. Ritonavir: Clinical  
599 Pharmacokinetics and Interactions with Other Anti-HIV Agents. *Clin Pharmacokinet* 35, 275–  
600 291.

601 Jamei, M., Abrahamsson, B., Brown, J., Bevernage, J., Bolger, M.B., Heimbach, T., Karlsson, E.,  
602 Kotzagiorgis, E., Lindahl, A., McAllister, M., Mullin, J.M., Pepin, X., Tistaert, C., Turner, D.B.,  
603 Kesisoglou, F., 2020. Current status and future opportunities for incorporation of dissolution  
604 data in PBPK modeling for pharmaceutical development and regulatory applications: OrBiTo  
605 consortium commentary. *Eur. J. Pharm. Biopharm.* 155, 55–68.  
606 <https://doi.org/10.1016/j.ejpb.2020.08.005>

607 Jamei, M., Turner, D., Yang, J., Neuhoff, S., Polak, S., Rostami-Hodjegan, A., Tucker, G., 2009.  
608 Population-based mechanistic prediction of oral drug absorption. *AAPS J.* 11, 225–237.  
609 <https://doi.org/10.1208/s12248-009-9099-y>

610 Jankovic, S., O' Dwyer, P.J., Box, K.J., Imanidis, G., Reppas, C., Kuentz, M., 2019. Biphasic drug release  
611 testing coupled with diffusing wave spectroscopy for mechanistic understanding of solid  
612 dispersion performance. *Eur. J. Pharm. Sci.* 137. <https://doi.org/10.1016/j.ejps.2019.105001>

613 Klein, S., Shah, V.P., 2008. A standardized mini paddle apparatus as an alternative to the standard  
614 paddle. *AAPS PharmSciTech* 9, 1179–84. <https://doi.org/10.1208/s12249-008-9161-6>

615 Koudriakova, T., Iatsimirskaia, E., Utkin, I., Gangl, E., Vouros, P., Storozhuk, E., Orza, D., Marinina, J.,  
616 Gerber, N., Ohio, T., 1998. Indinavir and ritonavir by human intestinal microsomes and  
617 expressed cytochrome p450 3A4/3A5 : mechanism-based inactivation of cytochrome p4503A  
618 by ritonavir. *DRUG Metab. Dispos.* 26, 552–561.

619 Kourentas, A., Vertzoni, M., Barmpatsalou, V., Augustijns, P., Beato, S., Butler, J., Holm, R.,  
620 Ouwerkerk, N., Rosenberg, J., Tajiri, T., Tannergren, C., Symillides, M., Reppas, C., 2018. The  
621 BioGIT System: a Valuable In Vitro Tool to Assess the Impact of Dose and Formulation on Early  
622 Exposure to Low Solubility Drugs After Oral Administration. *AAPS J.* 20, 71.  
623 <https://doi.org/10.1208/s12248-018-0231-8>

624 Kourentas, A., Vertzoni, M., Stavrinoudakis, N., Symillides, A., Brouwers, J., Augustijns, P., Reppas, C.,  
625 Symillides, M., 2016. An in vitro biorelevant gastrointestinal transfer (BioGIT) system for  
626 forecasting concentrations in the fasted upper small intestine: Design, implementation, and  
627 evaluation. *Eur. J. Pharm. Sci.* 82, 106–114. <https://doi.org/10.1016/j.ejps.2015.11.012>

628 Litou, C., Patel, N., Turner, D.B., Kostewicz, E., Kuentz, M., Box, K.J., Dressman, J., 2019. Combining

629 biorelevant in vitro and in silico tools to simulate and better understand the in vivo  
630 performance of a nano-sized formulation of aprepitant in the fasted and fed states. *Eur. J.*  
631 *Pharm. Sci.* 138, 105031. <https://doi.org/10.1016/j.ejps.2019.105031>

632 Litou, C., Turner, D.B., Holmstock, N., Ceulemans, J., Box, K.J., Kostewicz, E., Kuentz, M., Holm, R.,  
633 Dressman, J., 2020. Combining biorelevant in vitro and in silico tools to investigate the in vivo  
634 performance of the amorphous solid dispersion formulation of etravirine in the fed state. *Eur.*  
635 *J. Pharm. Sci.* 105297. <https://doi.org/https://doi.org/10.1016/j.ejps.2020.105297>

636 Litou, C., Vertzoni, M., Goumas, C., Vasdekis, V., Xu, W., Kesisoglou, F., Reppas, C., 2016.  
637 Characteristics of the Human Upper Gastrointestinal Contents in the Fasted State Under Hypo-  
638 and A-chlorhydric Gastric Conditions Under Conditions of Typical Drug – Drug Interaction  
639 Studies. *Pharm. Res.* 33, 1399–1412. <https://doi.org/10.1007/s11095-016-1882-8>

640 Litou, C., Vertzoni, M., Xu, W., Kesisoglou, F., Reppas, C., 2017. The impact of reduced gastric acid  
641 secretion on dissolution of salts of weak bases in the fasted upper gastrointestinal lumen : Data  
642 in biorelevant media and in human aspirates. *Eur. J. Pharm. Biopharm.* 115, 94–101.  
643 <https://doi.org/10.1016/j.ejpb.2017.02.009>

644 Markopoulos, C., Andreas, C.J., Vertzoni, M., Dressman, J., Reppas, C., 2015. In-vitro simulation of  
645 luminal conditions for evaluation of performance of oral drug products: Choosing the  
646 appropriate test media. *Eur. J. Pharm. Biopharm.* 93, 173–182.  
647 <https://doi.org/10.1016/j.ejpb.2015.03.009>

648 Marzo, A., Dal Bo, L., Verga, F., Ceppi Monti, N., Abbondati, G., Tettamanti, R. a, Crivelli, F., Uhr,  
649 M.R., Ismaili, S., 2000. Pharmacokinetics of diclofenac after oral administration of its potassium  
650 salt in sachet and tablet formulations. *Arzneimittelforschung.* 50, 43–7.  
651 <https://doi.org/10.1055/s-0031-1300162>

652 McAllister, M., 2010. Dynamic Dissolution: A Step Closer to Predictive Dissolution Testing? *Mol.*  
653 *Pharm.* 7, 1374–1387. <https://doi.org/10.1021/mp1001203>

654 Miller, D.A., Keen, J.M., Brough, C., Ellenberger, D.J., Cisneros, M., Williams III, R.O., McGinity, J.W.,  
655 2016. Bioavailability enhancement of a BCS IV compound via an amorphous combination  
656 product containing ritonavir. *J. Pharm. Pharmacol.* 68, 678–691.  
657 <https://doi.org/10.1111/jphp.12478>

658 Morcos, P.N., Moreira, S.A., Navarro, M.T., Bech, N., Quatkemeyer, A., Smith, P.F., Brennan, B.J.,  
659 2014. Effect of meal and antisecretory agents on the pharmacokinetics of danoprevir/ritonavir  
660 in healthy volunteers. *J. Pharm. Pharmacol.* 66, 23–31. <https://doi.org/10.1111/jphp.12151>

661 Ng, J., Klein, C.E., Chui, Y.L., Awni, W.M., Morris, J.B., Podsadecki, T.J., Cui, Y., Bernstein, B., Kim, D.,  
662 2008. The effect of food on ritonavir bioavailability following administration of ritonavir 100 mg  
663 film-coated tablet in healthy adult subjects. *J. Int. AIDS Soc.* 11, P247.  
664 <https://doi.org/10.1186/1758-2652-11-S1-P247>

665 O’Dwyer, P.J., Imanidis, G., Box, K.J., Reppas, C., 2020. On the Usefulness of Two Small-Scale In Vitro  
666 Setups in the Evaluation of Luminal Precipitation of Lipophilic Weak Bases in Early Formulation  
667 Development. *Pharmaceutics* 12. <https://doi.org/10.3390/pharmaceutics12030272>

668 O’Dwyer, P.J., Litou, C., Box, K.J., Dressman, J.B., Kostewicz, E.S., Kuentz, M., Reppas, C., 2019. In  
669 vitro methods to assess drug precipitation in the fasted small intestine – a PEARRL review. *J.*  
670 *Pharm. Pharmacol.* 71. <https://doi.org/10.1111/jphp.12951>

671 Pathak, S.M., Ruff, A., Kostewicz, E.S., Patel, N., Turner, D.B., Jamei, M., 2017. Model-Based Analysis  
672 of Biopharmaceutic Experiments to Improve Mechanistic Oral Absorption Modeling: An

673 Integrated in Vitro in Vivo Extrapolation Perspective Using Ketoconazole as a Model Drug. *Mol.*  
674 *Pharm.* 14, 4305–4320. <https://doi.org/10.1021/acs.molpharmaceut.7b00406>

675 Pathak, S.M., Schaefer, K.J., Jamei, M., Turner, D.B., 2019. Biopharmaceutic IVIVE Mechanistic  
676 Modeling of Single- and Two-Phase In Vitro Experiments to Obtain Drug-Specific Parameters for  
677 Incorporation Into PBPK Models. *J. Pharm. Sci.* 108, 1604–1618.  
678 <https://doi.org/10.1016/j.xphs.2018.11.034>

679 Poulin, P., Theil, F., 2009. Development of a Novel Method for Predicting Human Volume of  
680 Distribution at Steady-State of Basic Drugs and Comparative Assessment With Existing  
681 Methods. *J. Pharm. Sci.* 98, 4941–4961. <https://doi.org/10.1002/jps>

682 Psachoulas, D., Vertzoni, M., Goumas, K., Kalioras, V., Beato, S., Butler, J., Reppas, C., 2011.  
683 Precipitation in and supersaturation of contents of the upper small intestine after  
684 administration of two weak bases to fasted adults. *Pharm. Res.* 28, 3145–3158.  
685 <https://doi.org/10.1007/s11095-011-0506-6>

686 Rowland, M., Tozer, T.N., 1995. *Clinical pharmacokinetics: concepts and applications*, 3rd ed.

687 Rubbens, J., Mols, R., Brouwers, J., Augustijns, P., 2018. Exploring gastric drug absorption in fasted  
688 and fed state rats. *Int. J. Pharm.* 548, 636–641. <https://doi.org/10.1016/J.IJPHARM.2018.07.017>

689 Segregur, D., Barker, R., Mann, J., Moir, A., Karlsson, E.M., Turner, D.B., Arora, S., Dressman, J., 2021.  
690 Evaluating the impact of acid-reducing agents on drug absorption using biorelevant in vitro  
691 tools and PBPK modeling - case example dipyridamole. *Eur. J. Pharm. Sci.* 160, 105750.  
692 <https://doi.org/10.1016/J.EJPS.2021.105750>

693 Segregur, D., Flanagan, T., Mann, J., Moir, A., Karlsson, E.M., Hoch, M., Carlile, D., Sayah-Jeanne, S.,  
694 Dressman, J., 2019. Impact of Acid-Reducing Agents on Gastrointestinal Physiology and Design  
695 of Biorelevant Dissolution Tests to Reflect These Changes. *J. Pharm. Sci.* 108, 3461–3477.  
696 <https://doi.org/10.1016/J.XPHS.2019.06.021>

697 Tang, W.E.I., Stearns, R.A., Kwei, G.Y., Iliff, S.A., Miller, R.R., Egan, M.A., Yu, N.X., Dean, D.C., Kumar,  
698 S., Shou, M., Lin, J.H., Baillie, T.A., Metabolism, D., 1999. Interaction of Diclofenac and  
699 Quinidine in Monkeys : Stimulation of Diclofenac Metabolism. *J. Pharmacol. Exp. Ther.* 291,  
700 1068–1074.

701 Van Den Abeele, J., Brouwers, J., Mattheus, R., Tack, J., Augustijns, P., 2016. Gastrointestinal  
702 Behavior of Weakly Acidic BCS Class II Drugs in Man - Case Study of Diclofenac Potassium. *J.*  
703 *Pharm. Sci.* 105, 687–696. <https://doi.org/10.1002/jps.24647>

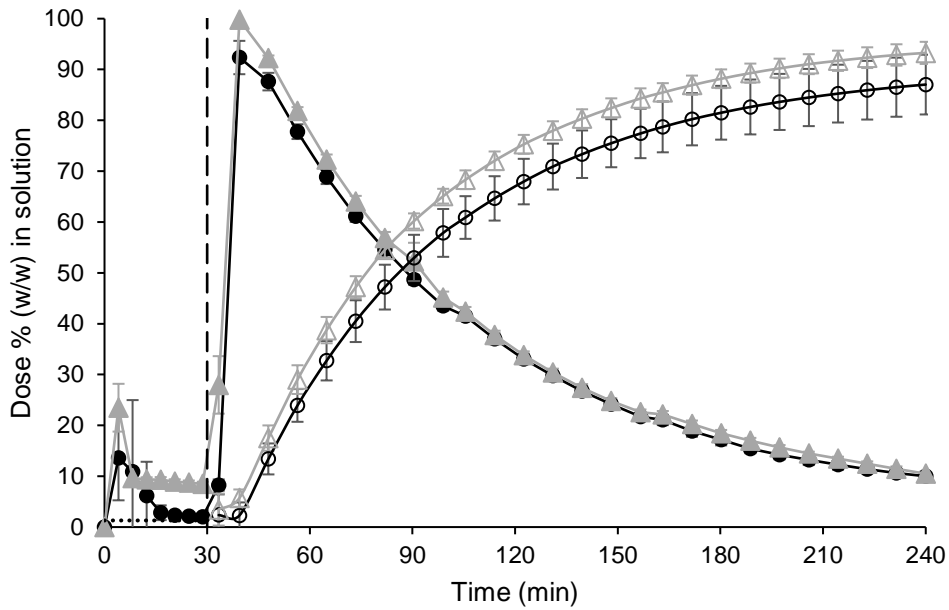
704 Van Den Abeele, J., Kostantini, C., Barker, R., Kourentas, A., Mann, J.C., Vertzoni, M., Beato, S.,  
705 Reppas, C., Tack, J., Augustijns, P., 2020. The effect of reduced gastric acid secretion on the  
706 gastrointestinal disposition of a ritonavir amorphous solid dispersion in fasted healthy  
707 volunteers: an in vivo - in vitro investigation. *Eur. J. Pharm. Sci.* 151.  
708 <https://doi.org/10.1016/j.ejps.2020.105377>

709 Van Den Abeele, J., Schilderink, R., Schneider, F., Mols, R., Minekus, M., Weitschies, W., Brouwers, J.,  
710 Tack, J., Augustijns, P., 2017. Gastrointestinal and Systemic Disposition of Diclofenac under  
711 Fasted and Fed State Conditions Supporting the Evaluation of in Vitro Predictive Tools. *Mol.*  
712 *Pharm.* 14, 4220–4232. <https://doi.org/10.1021/acs.molpharmaceut.7b00253>

713 Vidon, N., Pfeiffer, A., Godbillon, J., Rongier, M., Gauron, S., Hirtz, J., Bernier, J., Dubois, J., 1989.  
714 Evaluation of the gastric absorption and emptying of drugs under various pH conditions using a  
715 simple intubation method: application to diclofenac. *Br. J. Clin. Pharmacol.* 28, 121–124.  
716 <https://doi.org/10.1111/J.1365-2125.1989.TB03515.X>

- 717 Willis, J. V, Kendall, M.J., Flinn, R.M., Thornhill, D.P., Welling, P.G., 1979. The Pharmacokinetics of  
718 Diclofenac Sodium Following Intravenous and Oral Administration. *Eur. J. Clin. Pharmacol.* 16,  
719 405–410.
- 720 Wisdom Pharmaceutical Technology Co Limited, 2020. Voltfast Sachets 50mg Powder for Oral  
721 Solution Summary of Product Characteristics.
- 722 Xu, H., Vela, S., Shi, Y., Marroum, P., Gao, P., 2017. In Vitro Characterization of Ritonavir Drug  
723 Products and Correlation to Human in Vivo Performance. *Mol. Pharm.* 14, 3801–3814.  
724 <https://doi.org/10.1021/acs.molpharmaceut.7b00552>
- 725

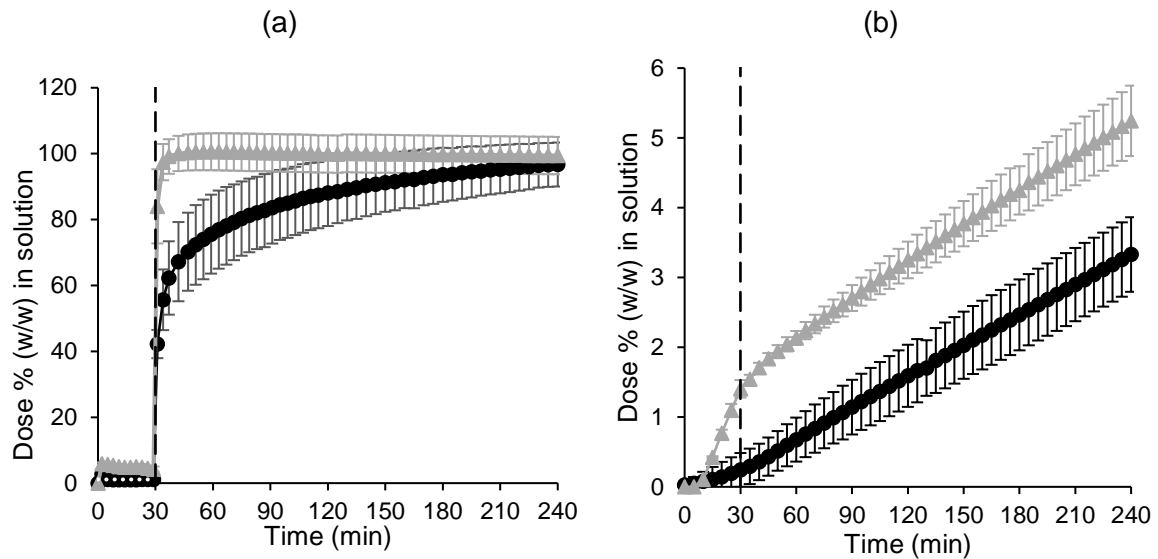
726 Figures



727

728 *Figure 1: Mean  $\pm$  SD (n = 3) diclofenac data from the small-scale two-stage biphasic system*  
729 *experiments. Percentage of dose (w/w) in solution in the aqueous and decanol layers are*  
730 *represented by the filled and hollow symbols, respectively. Cataflam<sup>®</sup> and Voltfast<sup>®</sup> data are*  
731 *represented by black circles and grey triangles, respectively. The dashed line indicates the time of*  
732 *transition from simulated gastric to simulated intestinal conditions. The horizontal dotted line*  
733 *corresponds to the equilibrium concentration of the free acid in dilute HCl (Guhmann et al., 2013)*  
734 *(converted to an equivalent percentage (w/w) of the dose).*

735



736 *Figure 2: Mean  $\pm$  SD (n = 3) diclofenac data from the small-scale two-stage D-P system experiments.*

737 *(a) Percentage of dose (w/w) in solution in the donor chamber; (b) Percentage of dose (w/w) in*

738 *solution in the acceptor chamber. The dashed line indicates the time of transition from simulated*

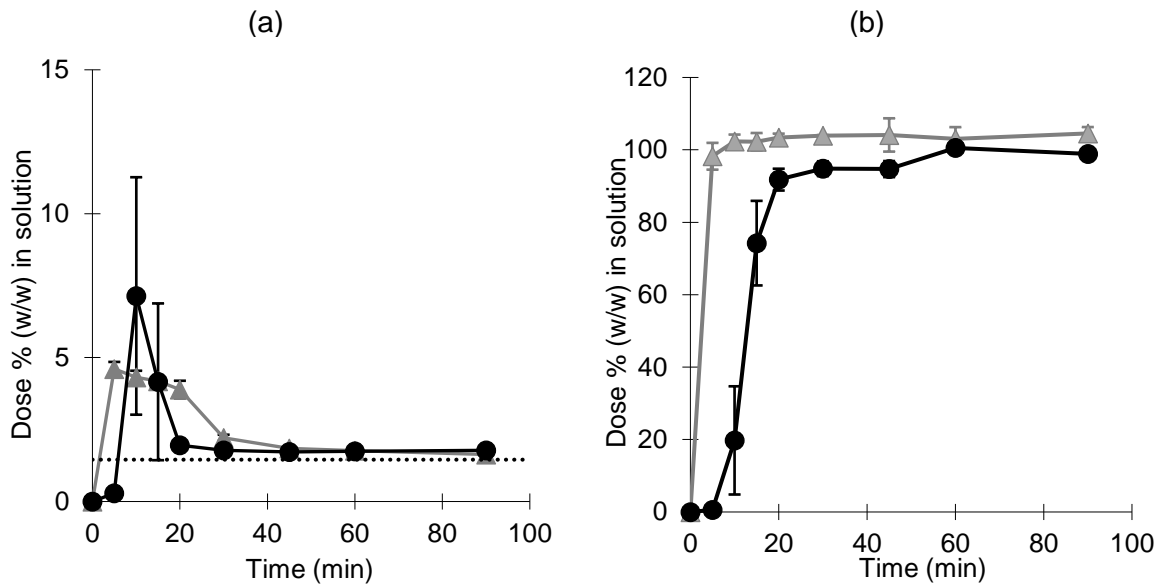
739 *gastric to simulated intestinal conditions. Cataflam® and Voltfast® data are represented by black*

740 *circles and grey triangles, respectively. The horizontal dotted line corresponds to the equilibrium*

741 *concentration of the free acid in dilute HCl (Guhmann et al., 2013) (converted to an equivalent*

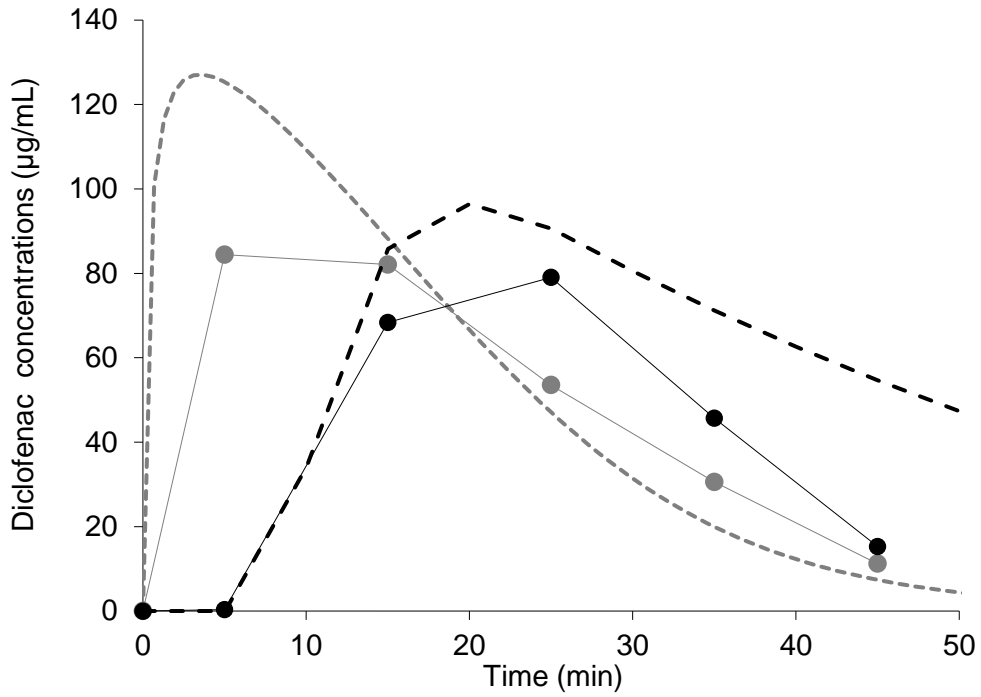
742 *percentage (w/w) of the dose).*

743



744 Figure 3: Mean  $\pm$  SD ( $n = 3$ ) percentage diclofenac dissolved (w/w) when using the Erweka mini-  
 745 paddle apparatus (75 rpm) in 250mL Level III FaSSGF (a) and in 250mL Level II FaSSIF (b). Cataflam®  
 746 and Voltfast® data are represented by black circles and grey triangles, respectively. The horizontal  
 747 dotted line corresponds to the equilibrium concentration of the free acid (converted to an equivalent  
 748 percentage (w/w) of the dose).

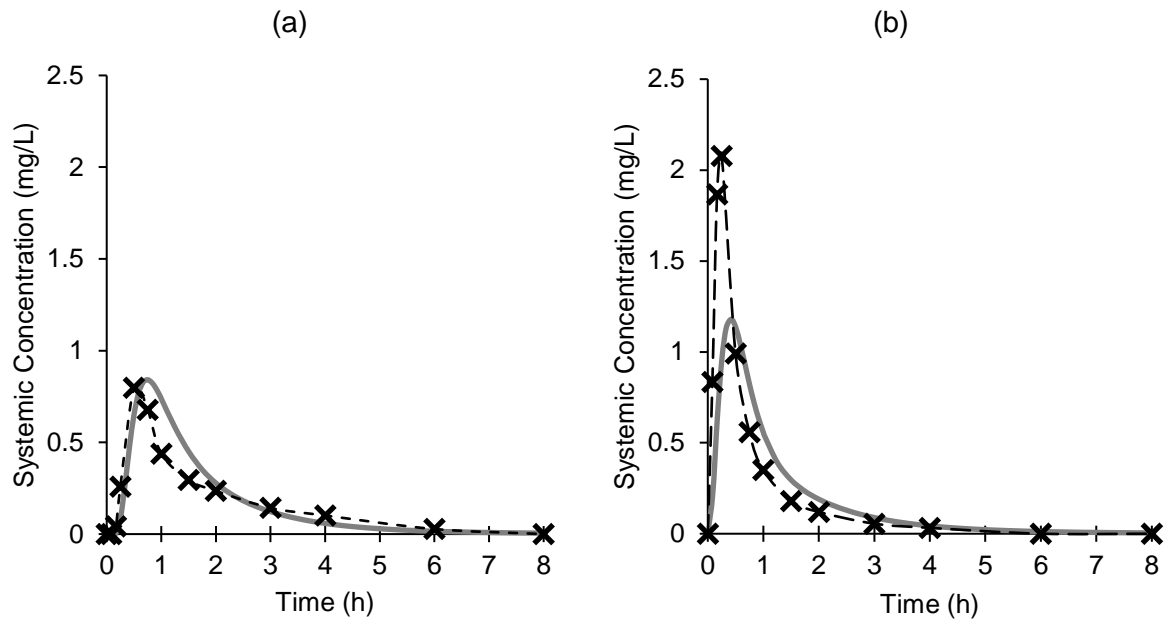
749



750

751 *Figure 4: Mean ± SD (n = 3) apparent diclofenac concentrations in the duodenal compartment of*  
 752 *BioGIT (-•-) and simulated duodenal profiles using PBB modelling (- - -) for Cataflam® (grey) and*  
 753 *Voltfast® (black).*

754

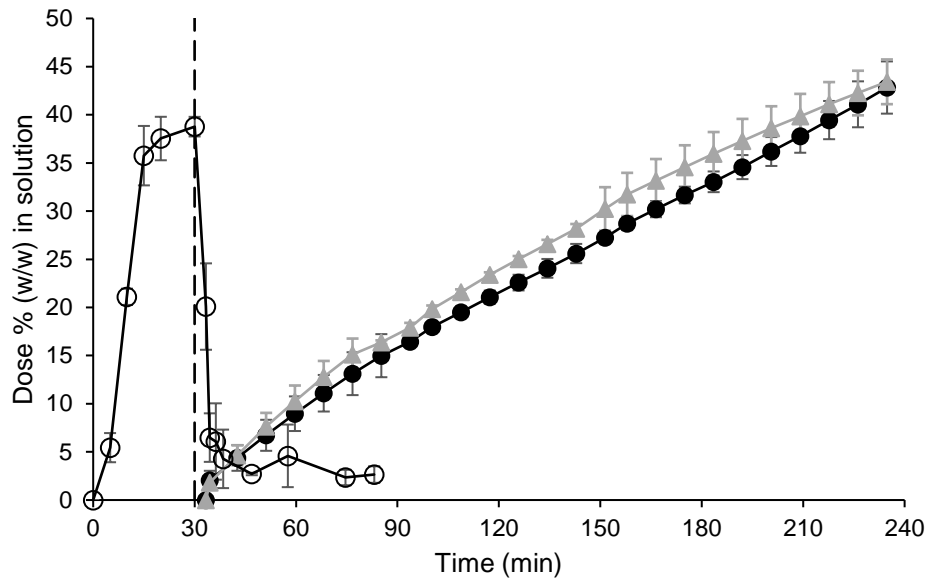


755 *Figure 5: Mean diclofenac plasma concentrations after single oral administration of Cataflam® (a)*  
 756 *and Voltfast® (b) to healthy adults in the fasted state (-x-); measures of variability were not reported*  
 757 *in the relevant reference (Marzo et al., 2000). Continuous lines are simulated plasma profiles using*  
 758 *PBB modelling.*

759

760

761



762

763

*Figure 6: Mean  $\pm$  SD (n = 3) ritonavir data from the small-scale two-stage biphasic system*

764

*experiments. Percentage of dose (w/w) in solution in the aqueous and decanol layers are*

765

*represented by the filled and hollow symbols, respectively. Simulated normal gastric and*

766

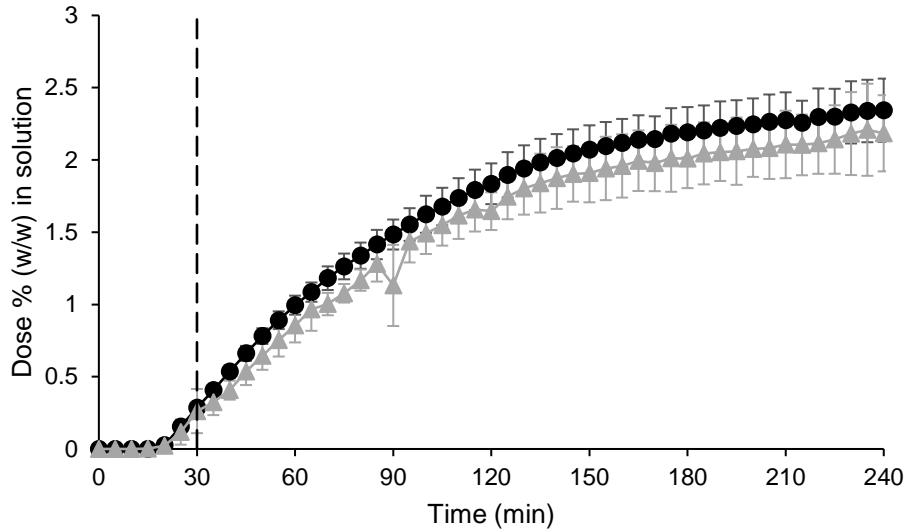
*hypochlorhydric conditions are represented by black circles and grey triangles, respectively. The*

767

*dashed line indicates the time of transition from simulated gastric to simulated intestinal conditions.*

768

769

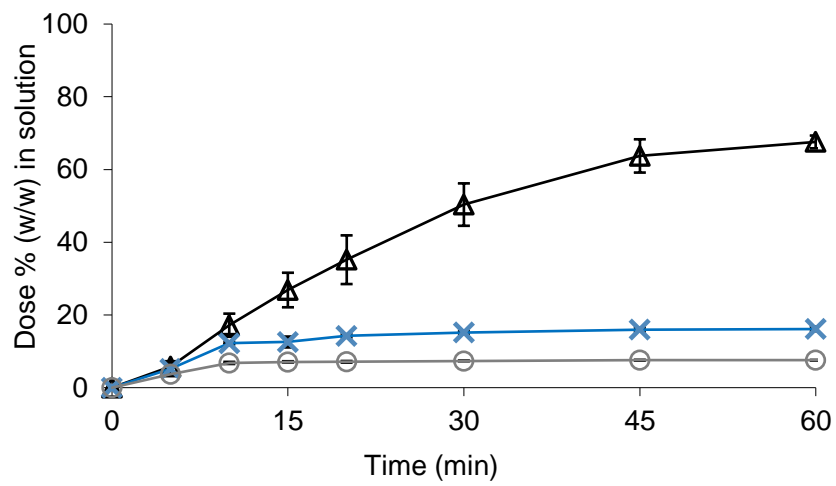


770

771 *Figure 7: Mean  $\pm$  SD (n = 3) percentage of ritonavir (w/w) in solution in the acceptor chamber of the*  
 772 *small-scale two-stage D-P system. The dashed line indicates the time of transition from simulated*  
 773 *gastric to simulated intestinal conditions. Simulated normal and hypochlorhydric gastric conditions*  
 774 *are represented by black circles and grey triangles, respectively.*

775

776



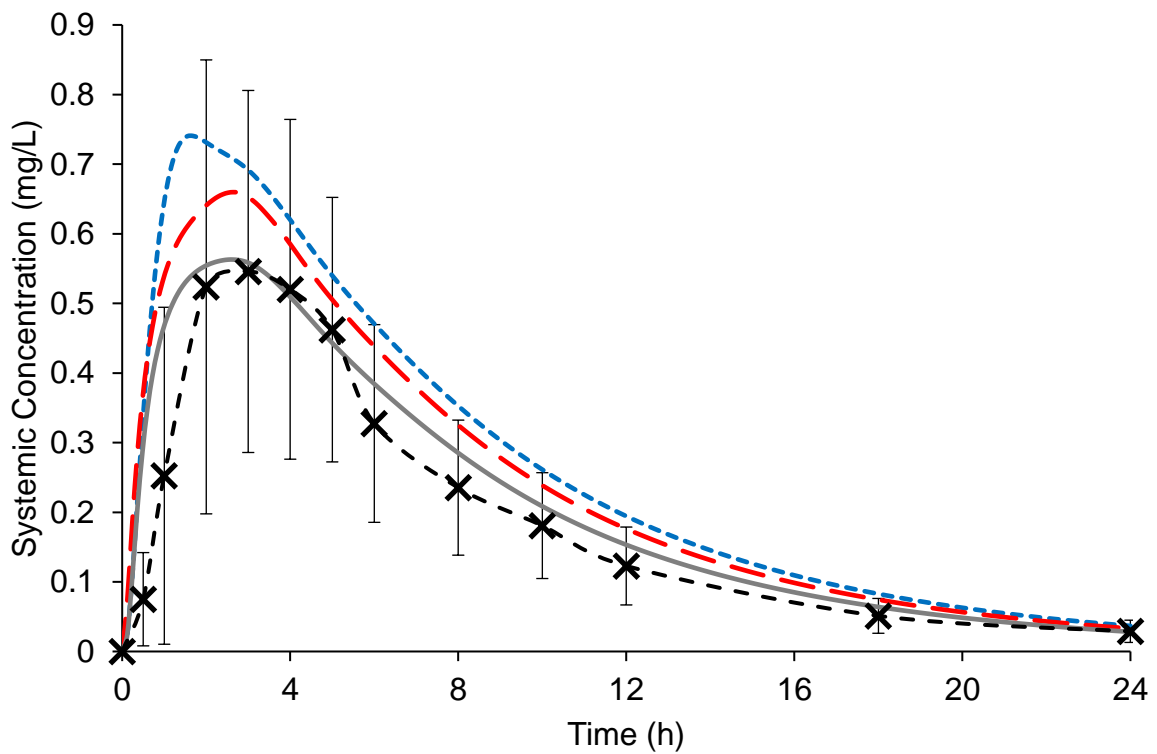
777

778 *Figure 8: Mean  $\pm$  SD (n = 3) percentage of ritonavir dissolved (w/w) from Norvir<sup>®</sup> in 250mL Level III*

779 *FaSSGF ( $\Delta$ ), 250mL Level III hypochlorhydric FaSSGF ( $\circ$ ), and 250mL Level II FaSSIF (x) when using the*

780 *Erweka mini-paddle apparatus (75 rpm).*

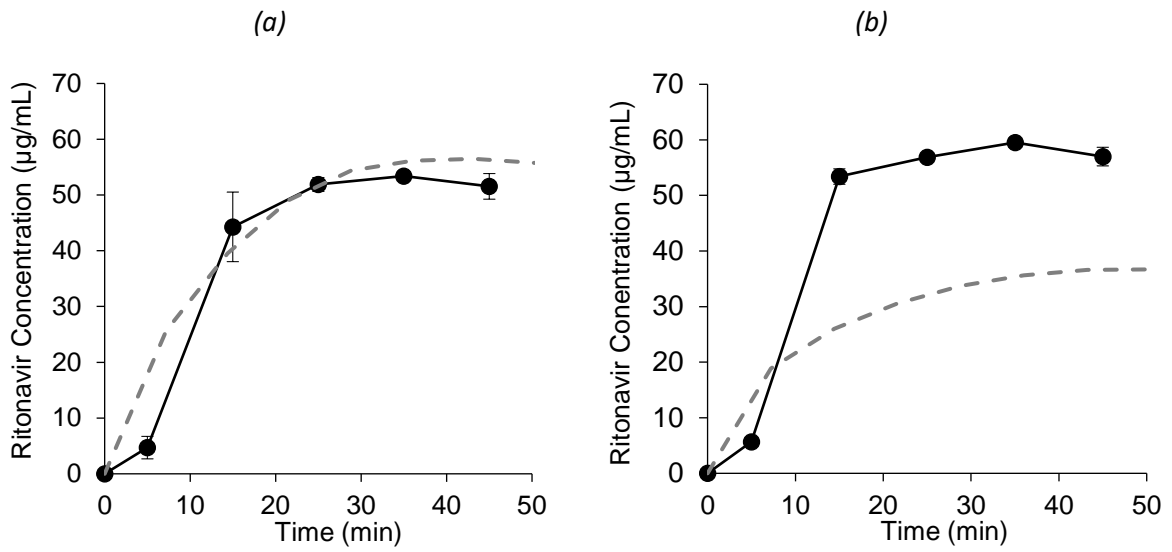
781



783

784 *Figure 9: Mean ( $\pm$  SD) ritonavir plasma concentrations after single dose administrations of one*  
 785 *Norvir® tablet to fasted healthy adults (Ng et al., 2008) vs. simulated ritonavir plasma profiles using*  
 786 *PBB modelling and the experimentally determined DLM scalar value (no precipitation) i.e., using the*  
 787 *Erweka mini-paddle apparatus data (blue dotted line), the experimentally determined PRC & default*  
 788 *DLM scalar value i.e., the small-scale two-stage biphasic system data (red dashed line), and the*  
 789 *experimentally determined PRC & DLM scalar values i.e., using both Erweka mini-paddle apparatus*  
 790 *and small-scale two-stage biphasic system data (solid grey line).*

791



793 *Figure 10: Mean  $\pm$  SD ( $n = 3$ ) apparent ritonavir concentrations in the duodenal compartment of*  
 794 *BioGIT (-•-) (reproduced from Van Den Abeele et al. 2020) and simulated ritonavir duodenal profiles*  
 795 *using PBB modelling (- - -) assuming that one Norvir<sup>®</sup> tablet is administered under normal (a) and*  
 796 *hypochlorhydric (b) gastric conditions.*

## 797 Tables

798 Table 1: Values of Physicochemical and Pharmacokinetic parameters used in the PBB modelling for  
799 diclofenac.

Parameter (units)	Values used	References/comments
<b>Physicochemical and blood binding parameters</b>		
Molecular weight (g/mol)	296.15	
Log Po:w	4.4	(Chuasuan et al., 2009)
Compound type	Monoprotic acid	(Chuasuan et al., 2009)
pKa	3.8	(Chuasuan et al., 2009)
Fraction unbound in plasma	0.003	(Accord-UK Ltd, 2018)
Blood plasma ratio	0.7	(Tang et al., 1999)
Fraction unbound in enterocyte	1	Simcyp compound file
<b>Drug absorption parameters (ADAM model)</b>		
MechPeff Model $P_{trans,0}$ ( $10^{-6}$ cm/s)	440108.3	Predicted using physicochemical properties
Predicted $P_{eff,man}$ ( $10^{-4}$ cm/s)	3.89 (duodenum), 10.06 (jejunum I), 7.05 (jejunum II), 1.65 (Ileum I), 1.65 (Ileum II), 1.62 (Ileum III), 1.56 (Ileum IV), 0.85 (colon)	Predicted in Simcyp using Mechpeff Model
Aqueous intrinsic solubility (mg/mL)	0.0018	Calculated used pH solubility profile (Guhmann et al., 2013)
Solubility factor	546.20	Estimated in Simcyp
Particle density (g/mL)	1.2	Default Simcyp Value
Particle size distribution	Monodispersed	Default Simcyp Value
Particle radius ( $\mu$ m)	10	Default Simcyp Value
Log bile micellar: buffer partition coefficient (Log $K_{m,w}$ ) neutral	5.91	Estimated in SIVA
Log $K_{m,w}$ ion	0.00038	Estimated in SIVA
Particle diffusion layer thickness ( $h_{eff}$ ) prediction	Hintz-Johnson method	
Monomer diffusion coefficient ( $10^{-4}$ cm <sup>2</sup> /min)	4.73	Predicted in Simcyp
Micelle diffusion coefficient ( $10^{-4}$ cm <sup>2</sup> /min)	0.78	Default Simcyp value
Diffusion layer model (DLM) Scalar (tablet formulation)	31.13	Estimated in SIVA from Erweka mini-paddle dissolution experiment
Disintegration Model	First order	
Maximum % fraction of drug dose dissolved	100	Estimated in SIVA from Erweka mini-paddle dissolution experiment
Kd1	0.17	
Lag (min)	7.43	
<b>Distribution parameters</b>		
Model	Minimal PBPK model	
$k_{in}$ (1/h)	1.88	Estimated using IV data
$k_{out}$ (1/h)	1.48	Estimated using IV data
$V_{sac}$ (L/kg)	0.11	Estimated using IV data
Method	Method 2	
Tissue-plasma partition coefficient (Kp) scalar	2	(Davies and Anderson, 1997)
Steady State Volume of Distribution ( $V_{ss}$ ) (L/kg)	0.15	Predicted within Simcyp
<b>Elimination parameters</b>		
Intravenous clearance ( $CL_{iv}$ ) (L/h)	21.50	Estimated using IV data
Renal clearance (L/h)	0.00036	(Rowland and Tozer, 1995)
<b>Population parameters</b>		
Stomach Mean residence time (h)	0.27 (Tablet) / 0.05 (Solution)	

801 *Table 2: Values of Physicochemical and Pharmacokinetic parameters used in the PBB modelling for*  
 802 *ritonavir.*

Parameter (units)	Values used	References/comments
<b>Physicochemical and blood binding parameters</b>		
Molecular weight (g/mol)	720.9	
Log Po:w	4.3	In house experimental database
Compound type	Diprotic Base	In house experimental database
pKa	1.8, 2.6	In house experimental database
Fraction unbound in plasma	0.005	(Denissen et al., 1997)
Blood plasma ratio	0.66	Predicted in Simcyp
Fraction unbound in enterocyte	1	Simcyp compound file
<b>Drug absorption parameters (ADAM Model)</b>		
MechPeff Model $P_{trans,0}$ ( $10^{-6}$ cm/s)	1465.85	Predicted using physicochemical properties
Predicted $P_{eff,man}$ ( $\times 10^{-4}$ cm/s)	2.84 (duodenum), 7.56 (jejunum I), 5.30 (jejunum II), 1.15 (Ileum I), 1.15 (Ileum II), 1.13 (Ileum III), 1.09 (Ileum IV), 0.59 (colon)	Predicted in Simcyp using Mechpeff Model
Aqueous intrinsic solubility (mg/mL)	0.061	Calculated using intestinal dissolution plateau values from the Erweka mini-paddle apparatus (this study)
Solubility factor	4.25	Estimated using the maximum concentrations observed in Erweka mini-paddle dissolution experiments
Particle density (g/mL)	1.2	Default Simcyp value
Particle size distribution	Monodispersed	Default Simcyp value
Particle radius ( $\mu$ m)	10	Default Simcyp value
Particle $h_{eff}$ prediction	Hintz-Johnson method	
Critical supersaturation ratio	1.00	Calculated from kinetic solubility data from solvent shift experiments (see section 3.2.4) and (Xu et al., 2017)
Precipitation rate constant (PRC) (1/h)	9.45	Calculated from biphasic experimental data. Note precipitation to amorphous state (Miller et al., 2016; Xu et al., 2017).
Monomer diffusion coefficient ( $10^{-4}$ cm <sup>2</sup> /min)	3.14	Predicted in Simcyp
Micelle diffusion coefficient ( $10^{-4}$ cm <sup>2</sup> /min)	0.78	Default Simcyp value
DLM Scalar	0.028 (stomach), 0.016 (hypochlorhydric stomach), 0.072 (intestine)	Estimated in SIVA from Erweka mini-paddle dissolution experiment. Note dissolution occurs of any solid drug, irrespective of origination as undissolved or precipitated drug
<b>Distribution parameters</b>		
Model	Full PBPK model	
Method	Method 2	
Kp scalar	0.06	(Hsu et al., 1998)
Vss (L/kg)	0.35	Predicted within Simcyp
<b>Elimination parameters</b>		
CYP2D6	0.7 (Vmax), 1.0 (Km)	Simcyp compound file
CYP3A4	1.37 (Vmax), 0.07 (Km)	Simcyp compound file with BD SUP ISEF (Intersystem extrapolation factor)
CYP3A5	1.0 (Vmax) 0.05 (Km)	Simcyp compound file with BD SUP ISEF
Renal clearance (L/h)	0.006	(Rowland and Tozer, 1995)

803

804

805 *Table 3: Values of pharmacokinetic parameters calculated from in vivo data (n = 24) (Marzo et al.,*  
 806 *2000) and estimated using PBB modelling (this study) for Cataflam® and Voltfast\*.*

	Cataflam®				Voltfast®			
	<i>In vivo data</i>	PBB model	FD	AAFE	<i>In vivo data</i>	PBB model	FD	AAFE
Mean AUC (mg.h/L)	1.21	1.32	1.09	1.55	1.36	1.38	1.01	1.80
Mean C <sub>max</sub> (mg/L)	1.07	0.93	0.87		2.21	1.19	0.54	
Median T <sub>max</sub> (h)	0.63	0.76	0.86		0.25	0.41	1.80	

807

808 AAFE: Absolute Average Fold Error; FD: fold difference predicted/observed

809

810 Table 4: Values of pharmacokinetic parameters calculated from *in vivo* data (n = 27) (Ng et al., 2008) and estimated using PBB modelling (this study) for  
 811 Norvir® 100 mg tablets.

	<i>In vivo</i> data	Default DLM scalar value & no precipitation			Experimentally derived DLM scalar value (no precipitation)			Experimentally derived PRC value (default DLM scalar value)			Experimentally derived PRC and DLM scalar values			Hypochlorhydric gastric conditions		
		PBB model	FD	AAFE	PBB model	FD	AAFE	PBB model	FD	AAFE	PBB model	FD	AAFE	PBB model	FD	AAFE
Mean AUC (mg.h/L)	4.7	14.45	3.07	3.52	6.29	1.34	1.50	5.71	1.22	1.37	4.76	1.01	1.26	4.43	0.94	N/A
Mean C <sub>max</sub> (mg/L)	0.60	2.07	3.44		0.74	1.24		0.68	1.13		0.56	0.93		0.52	0.87	
Mean T <sub>max</sub> (h)	3.2	1.06	0.33		1.53	0.48		2.19	0.68		2.16	0.68		2.35	0.73	

812

813 AAFE: Absolute Average Fold Error; FD: fold difference predicted/observed; PRC = Precipitation Rate Constant; DLM = Diffusion Layer Model

